Electronic Supplementary Material (ESI) for Journal of Materials Chemistry A.

Supporting information

$La(OH)_3$ nanosheet supported CoPt nanoparticles: Highly efficient and magnetically recyclable catalyst for hydrogen production from hydrous hydrazine

Kun Wang,[a] Qilu Yao,[a] Shaojun Qing[b] and Zhang-Hui Lu[a]*

[a]Institute of Advanced Materials, College of Chemistry and Chemical Engineering, Jiangxi Normal University, Nanchang, 330022, China; [b]Institute of Coal Chemistry, Chinese Academy of Sciences, Taiyuan, 030000, China

**Corresponding author: E-mail: luzh@jxnu.edu.cn*

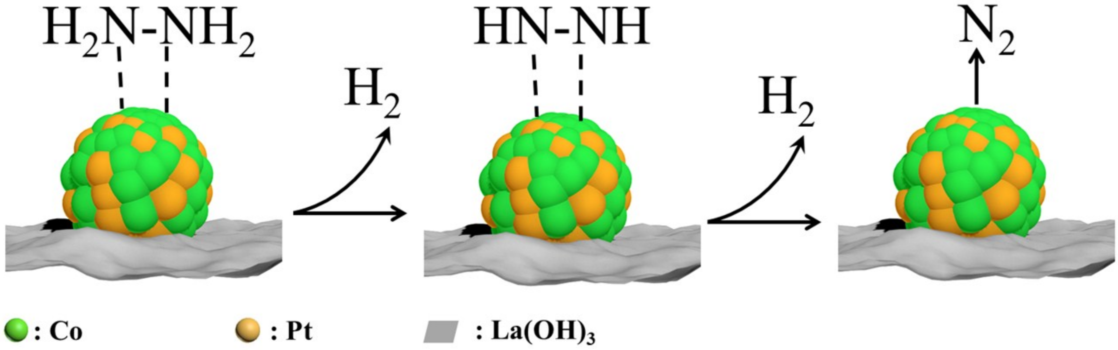

Scheme S1. The mechanism of N_2H_4 decoposition on CoPt NPs surface.

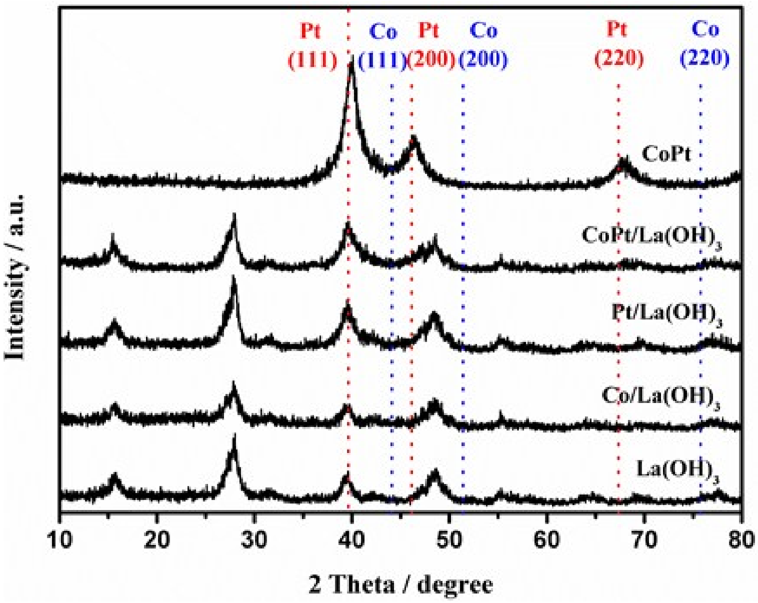

Fig. S1 Powder XRD patterns of the as-synthesized $La(OH)_3$, $Co/La(OH)_3$, $Pt/La(OH)_3$, $CoPt/La(OH)_3$, and free CoPt NPs

As shown in Fig. S1, four obvious characterized peaks located at 15.6°, 27.9°, 39.5° and 48.5° are observed in $CoPt/La(OH)_3$, which are assigned to hexagonal $La(OH)_3$ (PDF# 36-1481). No obvious peak belongs to CoPt NPs appears in $CoPt/La(OH)_3$, which can be explained as good dispersion of the ultrafine CoPt NPs on $La(OH)_3$ surface and/or superposition of CoPt and $La(OH)_3$ peaks. It is noted that the peak located at 39.5° is obviously enhanced in $CoPt/La(OH)_3$ and $Pt/La(OH)_3$ as compared to that of pure $La(OH)_3$ owing to the superposition of Pt (111) and $La(OH)_3$ peaks. To eliminate the disturbance of $La(OH)_3$, pure CoPt NPs were prepared for characterization. The XRD pattern of free CoPt NPs has a crystalline peak of CoPt alloy located at 39.9°, which is between the characteristic peaks of cubic Pt (111) plane (PDF# 04-0802) and cubic Co (111) plane (PDF# 15-0806).

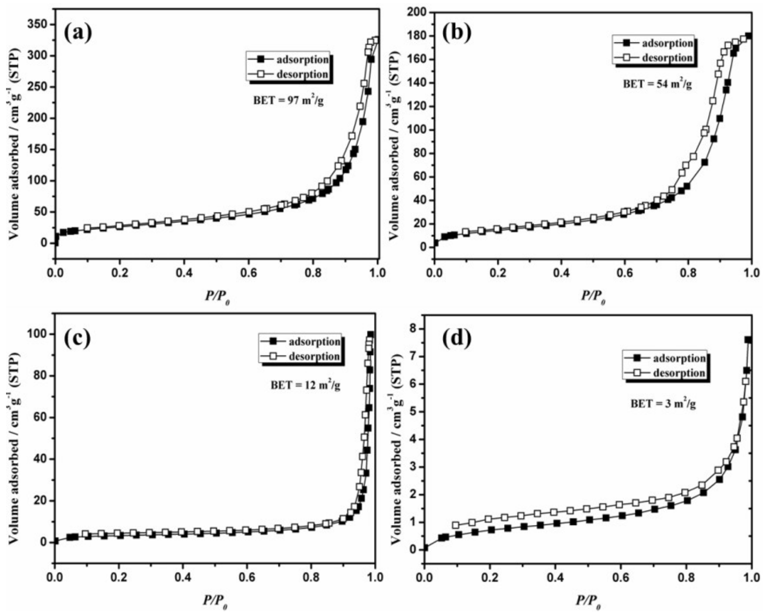

Fig. S2 Nitrogen adsorption−desorption isotherms of the (a) naonosheet-, (b) nanoshpere-, (c) nanorod-, (d) nanobelt-like $La(OH)_3$.

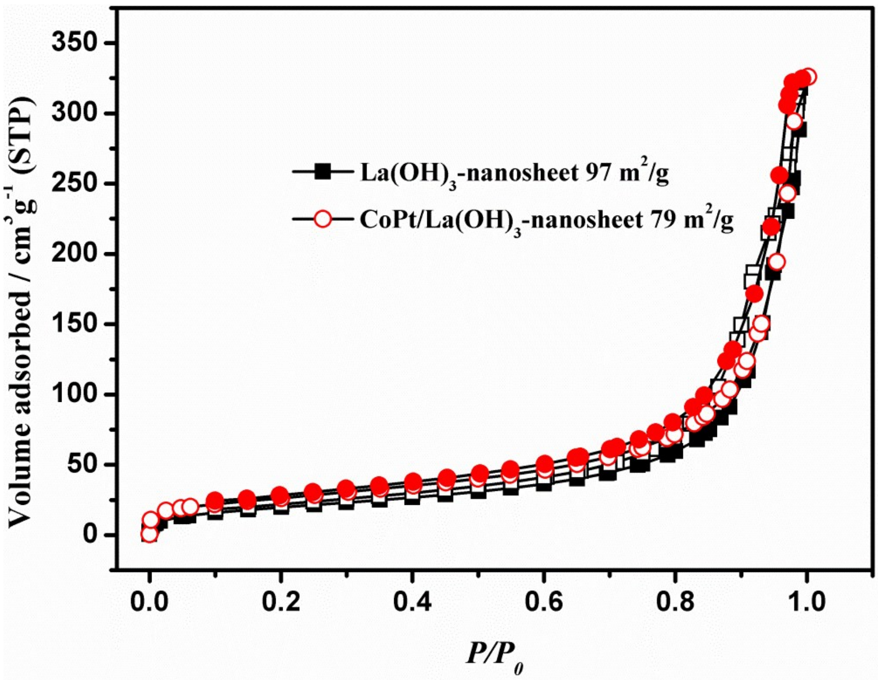

Fig. S3 Nitrogen adsorption−desorption isotherms of the CoPt/$La(OH)_3$-nanosheet and $La(OH)_3$-nanosheet.

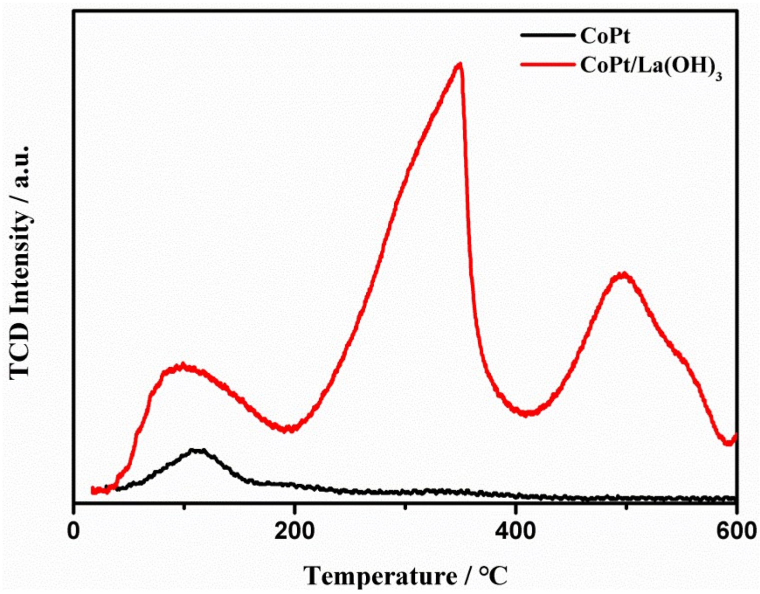

Fig. S4 CO_2-TPD mass spectra of the pure CoPt NPs and CoPt/La(OH)$_3$.

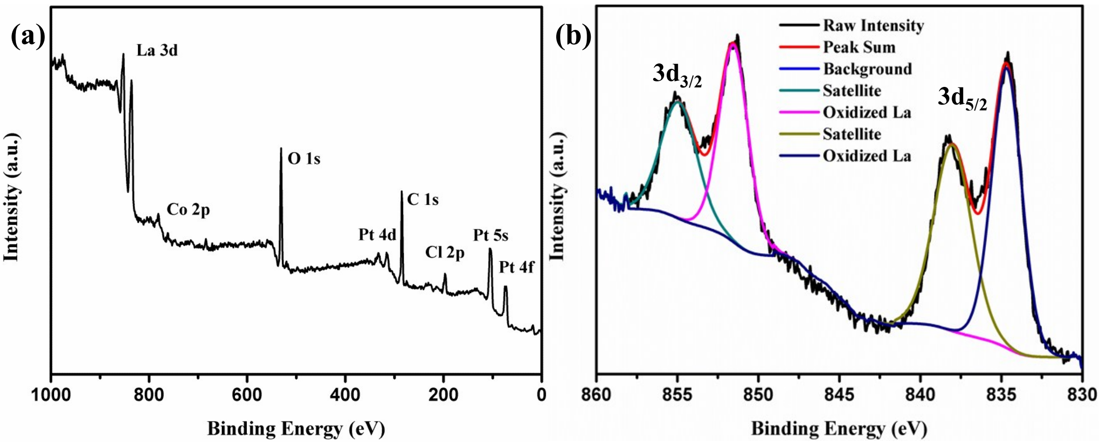

Fig. S5 (a) The survey XPS spectrum and (b) XPS spectrum of La 3d of $CoPt/La(OH)_3$.

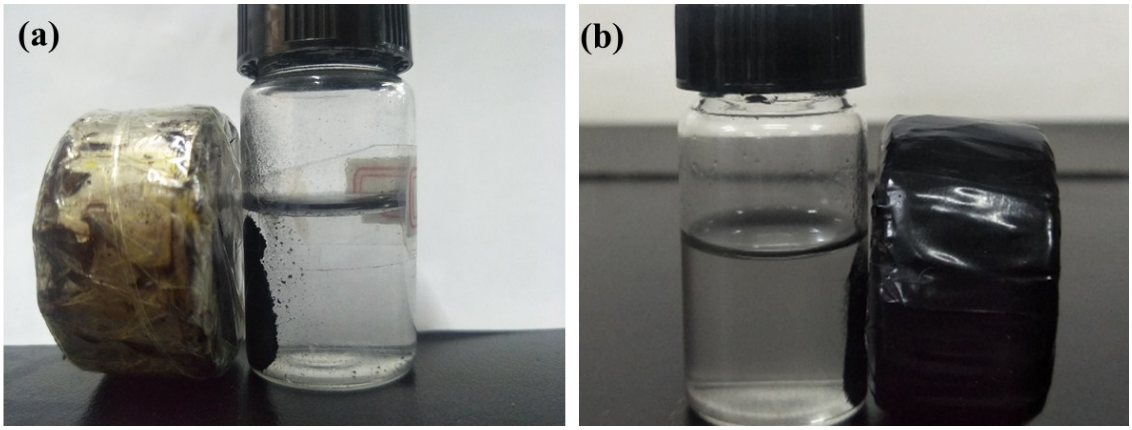

Fig. S6 Photograph of the (a) $CoPt/La(OH)_3$ and (b) after five recycle tests $CoPt/La(OH)_3$ after the magnetic separation.

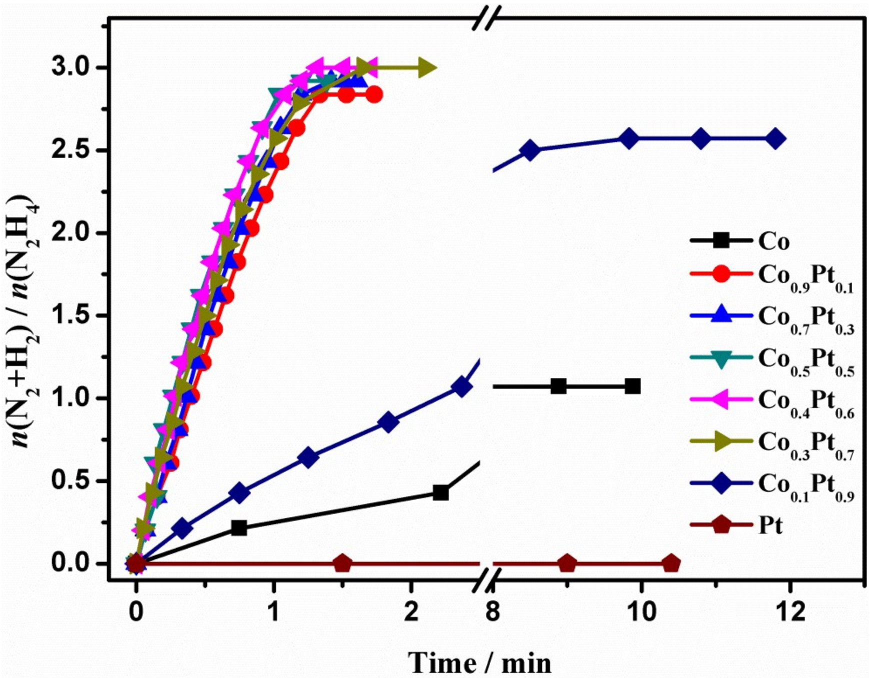

Fig. S7 Time course plots for decomposition of N_2H_4 (400 mM, 5 mL) over $CoPt/La(OH)_3$ with different molar contents of Pt in the presence of NaOH (3.5 M) at 323 K ($n_{CoPt}/n_{N_2H_4 \cdot H_2O} = 0.05$).

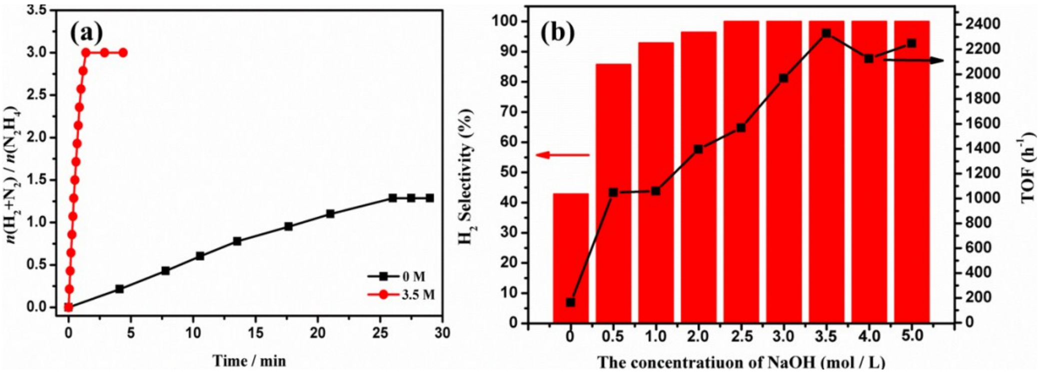

Fig. S8 (a) Time course plots and (b) NaOH dependence of H_2 selectivity and the corresponding TOF values for dehydrogenation of N_2H_4 (400 mM, 5 mL) over CoPt/La$(OH)_3$ with different amounts of NaOH at 323 K ($n_{CoPt}/n_{N_2H_4 \cdot H_2O}$ = 0.05).

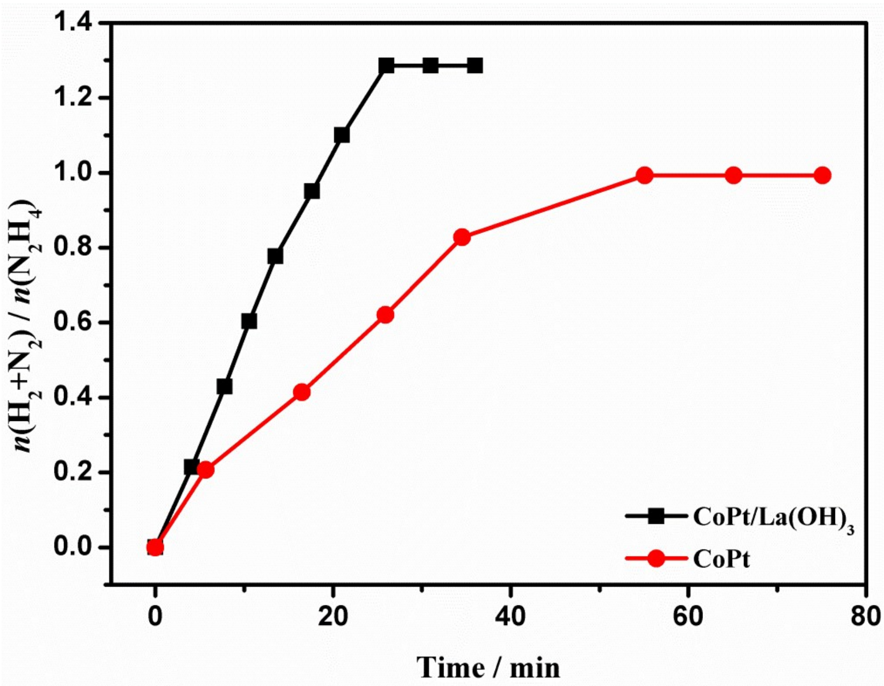

Fig. S9 Time course plots for decomposition of N_2H_4 (400 mM, 5 mL) over CoPt NPs and CoPt/La(OH)$_3$ without NaOH at 323 K ($n_{CoPt}/n_{N_2H_4 \cdot H_2O}$ = 0.05).

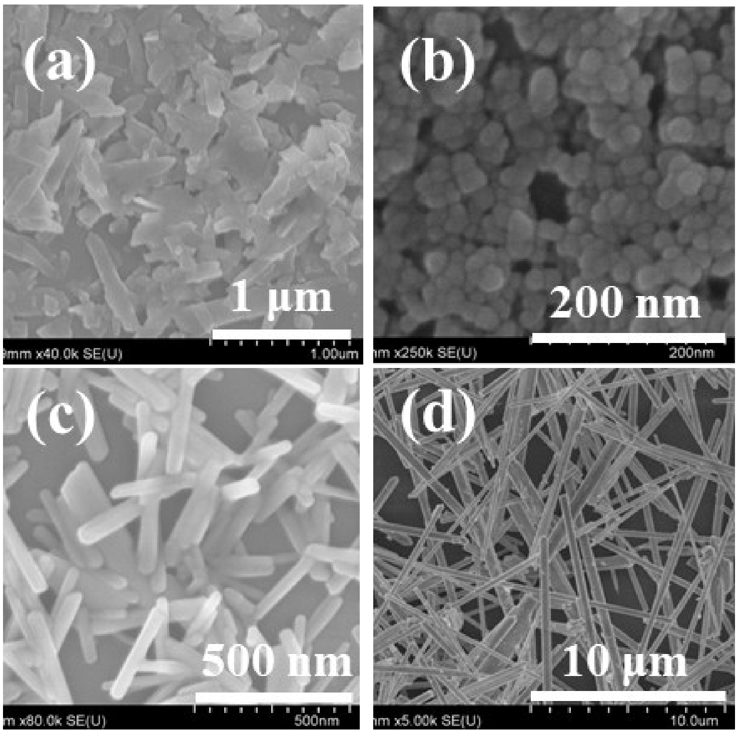

Fig. S10 Typical SEM images of the as-synthesized (a) naonosheet-, (b) nanoshpere-, (c) nanorod-, (d) nanobelt-like $La(OH)_3$.

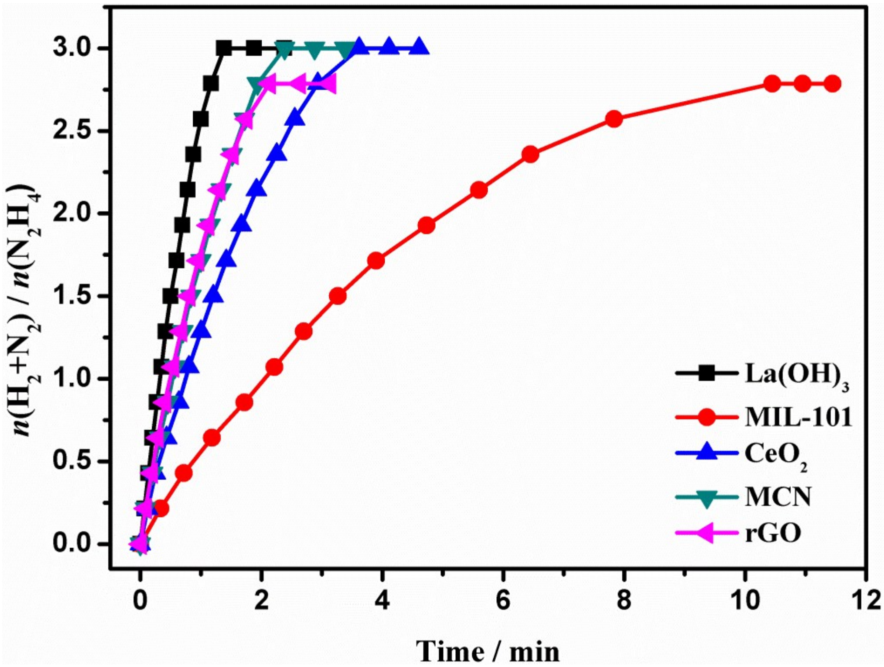

Fig. S11 Time course plots for decomposition of N_2H_4 (400 mM, 5 mL) over CoPt supported by different supports in the presence of NaOH (3.5 M) at 323 K ($n_{CoPt}/n_{N_2H_4 \cdot H_2O}$ = 0.05).

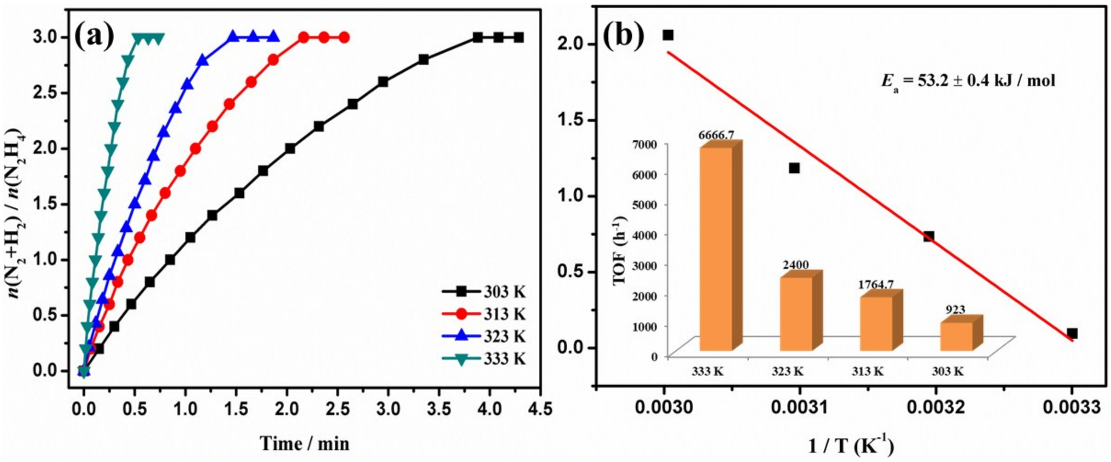

Fig. S12 (a) Time course plots for decomposition of N_2H_4 (400 mM, 5 mL) over NiPt/La(OH)$_3$ in the presence of NaOH (3.5 M) at different temperatures ($n_{NiPt}/n_{N_2H_4 \cdot H_2O}$ = 0.05); (b) The corresponding Arrhenius plot.

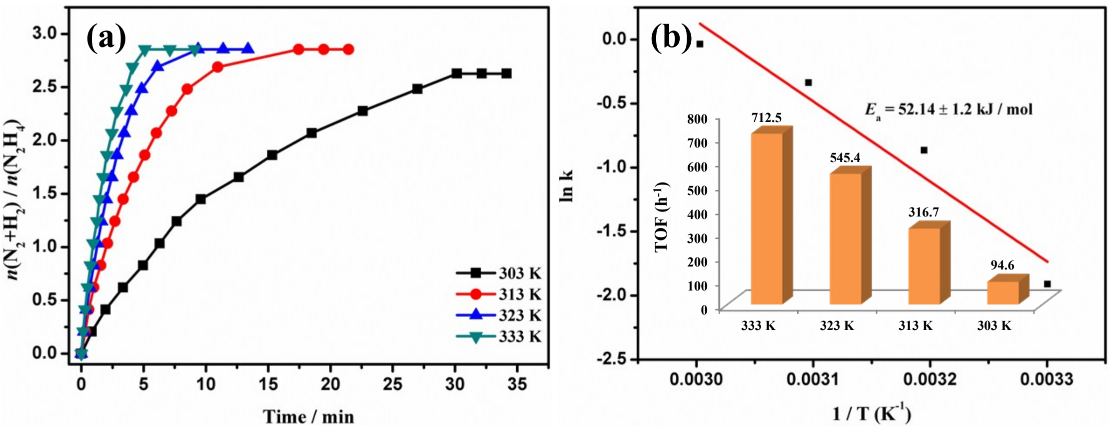

Fig. S13 (a) Time course plots for decomposition of N_2H_4 (400 mM, 5 mL) over pure CoPt NPs in the presence of NaOH (3.5 M) at different temperatures ($n_{CoPt}/n_{N_2H_4 \cdot H_2O}$ = 0.05); (b) The corresponding Arrhenius plot.

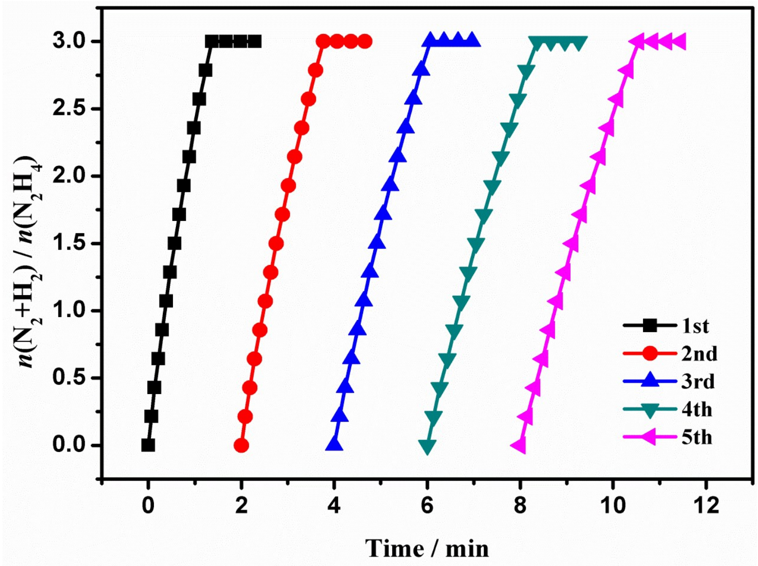

Fig. S14 Reusability test for decomposition of N_2H_4 (400 mM, 5 mL) over NiPt/La$(OH)_3$ with NaOH (3.5 M) at 323 K ($n_{NiPt}/n_{N_2H_4 \cdot H_2O}$ = 0.05).

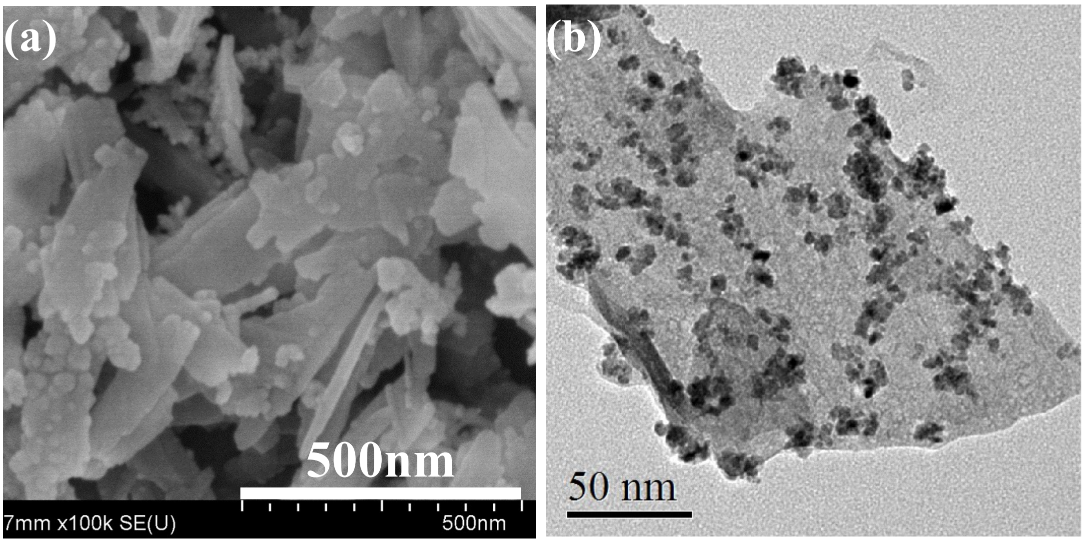

Fig. S15 Typical SEM (a) and TEM (b) image of the CoPt/La$(OH)_3$ after five runs.

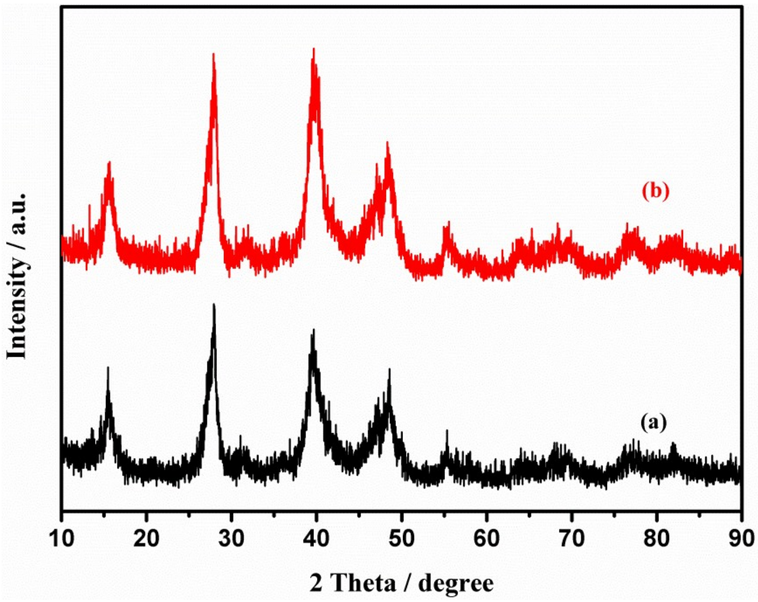

Fig. S16 Powder XRD patterns of the as-synthesized CoPt/La$(OH)_3$ catalyst (a) before and (b) after five runs.

Table S1 ICP-AES results of different catalysts.

Catalyst	Co (wt%)	Pt (wt%)	Co/Pt (molar ratio)
Co	12.47	-	-
$Co_{0.9}Pt_{0.1}$	11.79	4.38	8.89
$Co_{0.7}Pt_{0.3}$	8.00	11.51	2.29
$Co_{0.5}Pt_{0.5}$	5.73	15.62	1.02
$Co_{0.4}Pt_{0.6}$	4.32	21.64	0.65
$Co_{0.3}Pt_{0.7}$	3.01	23.90	0.42
$Co_{0.1}Pt_{0.9}$	1.02	30.55	0.11
Pt	-	32.77	-

Table S2. Catalytic activities of different catalysts for the dehydrogenation of hydrous hydrazine.

Catalyst	Temp. (K)	Selectivity (100%)	TOF (h^{-1})	E_a (kJ / mol)	Ref.
NiPt/Ce_2O_3	298	100	28.1	42.3	S1
NiPt/MIL-101	303	100	140	48.4	S2
NiPt/PDA-rGO	303	100	903	33.39	S3
NiCo/NiO-CoO_x	295	99	5.49	45.2	S4
$Co_{0.65}Pt_{0.30}(CeO_x)_{0.05}$	298	72.1	194.8	-	S5
CoIr/γ-Al_2O_3	298	100	27.76	40.8	S6
NiMoB-La$(OH)_3$	323	100	13.3	55.1	S7
$Pt_{0.5}Ni_{0.5}$/NGNs-850	323	100	2116	32.28	S8
$Ni_{84}Pt_{16}$/graphene	323	100	415	40.4	S9
Ni_3Pt_7/graphene	323	100	415	49.36	S10
$Rh_{4.4}Ni$/graphene	298	100	28	-	S11
$Pt_{60}Ni_{40}$-CNDs	323	100	170	43.9	S12
$NiIr_{0.059}$/Al_2O_3-HT	303	99	12.4	49.3	S13
$NiPt_{0.057}$/ Al_2O_3-HT	303	97	16.5	34	S14
$Ni_{1.5}Fe_{1.0}/(MgO)_{3.5}$	299	99	11	-	S15

PtNi/C	323	100	210	55.3	S16
NiPt/La(OH)$_3$	303	100	923	53.2	This work
NiPt/La(OH)$_3$	323	100	2400	53.2	This work
CoPt/La(OH)$_3$	303	100	734.2	45.2	This work
CoPt/La(OH)$_3$	323	100	2400	45.2	This work

References

(S1) H. L. Wang, J. M. Yan, Z. L. Wang, O. Song-Il and Q. Jiang, *J. Mater. Chem. A*, 2013, **1***,* 14957-14962.

(S2) Z. J. Zhang, S. L. Zhang, Q. L. Yao, X. S. Chen and Z. H. Lu, *Inorg. Chem.*, 2017, **56***,* 11938-11945.

(S3) F. Z. Song, Q. L. Zhu and Q. Xu, *J. Mater. Chem. A*, 2015, **3**, 23090-23094.

(S4) D. D. Wu, M. Wen, X. J. Lin, Q. S. Wu, C. Gu and H. X. Chen, *J. Mater. Chem. A*, 2016, **4***,* 6595-6602.

(S5) O. Song-Il, J. M. Yan, H. L. Wang, Z. L. Wang and Q. Jiang, *Int. J. Hydrogen Energy*, 2014, **39**, 3755-3761.

(S6) N. Firdous, N. K. Janjua, I. Qazi and M. H. Sarwar Wattoo, *Int. J. Hydrogen Energy*, 2016, **4**, 984-955.

(S7) J. Zhang, Q. Kang, Z. Yang, H. Dai, D. Zhuang and P. Wang, *J. Mater. Chem. A*, 2013, **1**, 11623-11628.

(S8) A. Kumar, X. C. Yang and Q. Xu, *J. Mater. Chem. A*, 2018, 10.1039/C8TA09003C.

(S9) Y. S. Du, J. Su, W. Luo and G. Z. Cheng, *ACS Appl. Mater. Interfaces*, 2015, **7**, 1031-1034.

(S10) N. Cao, L. Yang, C. Du, J. Su, W. Luo and G. Z. Cheng, *J. Mater. Chem. A*, 2014, **2**, 14344-14347.

(S11) J. Wang, X. B. Zhang, Z. L. Wang, L. M. Wang and Y. Zhang, *Energy Environ. Sci.*, 2012, **5**, 6885-6888.

(S12) J. K. Sun and Q. Xu, *ChemCatChem*, 2015, **7**, 526-531.

(S13) L. He, Y. Q. Huang, X. Y. Liu, L. Li, A. Q. Wang, X. D. Wang, Y. C. Mou and T. Zhang, *Appl. Catal. B*, 2014, **147**, 779-788.

(S14) L. He, Y. Q. Huang, A. Q. Wang, Y. Liu, X. Y. Liu, X. W. Chen, J. J. Delgado, X. D. Wang and T. Zhang, *J. Catal.*, 2013, **298**, 1-9.

(S15) W. Gao, C. M. Li, H. Chen, M. Wu, S. He, M. Wei, D. G. Evans and X. Duan, *Green Chem.*, 2014, **16**, 1560-1568.

(S16) S. N. Oliaee, C. L. Zhang, S. Y. Hwang, H. M. Cheung and Z. M. Peng, *J. Phys. Chem. C*, 2016, **120**, 9764-9772.